276 *Biochemistry* **2011,** *50,* 276–286
DOI: 10.1021/bi101511r

BIOCHEMISTRY
including biophysical chemistry & molecular biology
Article

Evidence That Ferredoxin Interfaces with an Internal Redox Shuttle in Acetyl-CoA Synthase during Reductive Activation and Catalysis†

Güneş Bender and Stephen W. Ragsdale*

Department of Biological Chemistry, University of Michigan, Ann Arbor, Michigan 48109, United States

Received September 16, 2010; Revised Manuscript Received December 8, 2010

ABSTRACT: Acetyl-CoA synthase (ACS), a subunit of the bifunctional CO dehydrogenase/acetyl-CoA synthase (CODH/ACS) complex of *Moorella thermoacetica* requires reductive activation in order to catalyze acetyl-CoA synthesis and related partial reactions, including the CO/[1-^{14}C]-acetyl-CoA exchange reaction. We show that the *M. thermoacetica* ferredoxin(II) (Fd-II), which harbors two [4Fe-4S] clusters and is an electron acceptor for CODH, serves as a redox activator of ACS. The level of activation depends on the oxidation states of both ACS and Fd-II, which strongly suggests that Fd-II acts as a reducing agent. By the use of controlled potential enzymology, the midpoint reduction potential for the catalytic one-electron redox-active species in the CO/acetyl-CoA exchange reaction is −511 mV, which is similar to the midpoint reduction potential that was earlier measured for other reactions involving ACS. Incubation of ACS with Fd-II and CO leads to the formation of the NiFeC species, which also supports the role of Fd-II as a reductant for ACS. In addition to being a reductant, Fd-II can accept electrons from acetylated ACS, as observed by the increased intensity of the EPR spectrum of reduced Fd-II, indicating that there is a stored electron within an "electron shuttle" in the acetyl-Ni(II) form of ACS. This "shuttle" is proposed to serve as a redox mediator during activation and at different steps of the ACS catalytic cycle.

Moorella thermoacetica is a homoacetogenic bacterium that uses a variety of organic and inorganic molecules as electron donors/acceptors and produces acetic acid as the final product via the Wood−Ljungdahl pathway when growing on a number of diverse carbon sources including glucose and CO_2 (*1*, *2*). Various anaerobic bacteria and archaea use the Wood−Ljungdahl pathway to assimilate CO_2 or CO into cellular carbon as well as to use CO as a source of energy. The pathway contains two branches, one of which reduces CO_2 by six electrons to generate methyltetrahydrofolate (methyl-H_4folate) through the action of five enzymes. The methyl group is then transferred first to a corrinoid iron−sulfur protein (CFeSP) by a methyltransferase (MTr) catalyzed reaction to generate a methyl-Co(III) intermediate and then from the CFeSP to acetyl-CoA synthase (ACS)[1] apparently to form a methyl-Ni intermediate. The second branch involves reduction of CO_2 to CO by carbon monoxide dehydrogenase (CODH), transfer of CO through a channel to the active site of ACS, and the ACS-catalyzed synthesis of acetyl-CoA from the CO, the bound methyl group, and CoA. This reaction is rather complicated because it involves the generation of a single product, acetyl-CoA, from three substrates. Pulse−chase studies have shown that the methyl and carbonyl groups bind to ACS in a random manner before the strictly ordered binding of the third substrate, CoA (*3*).

In *M. thermoacetica*, CODH and ACS make up the two subunits of a ∼310 kDa $\alpha_2\beta_2$ heterotetrameric enzymatic machine. The ACS α-subunit has been cloned and overexpressed in an active form in *E. coli* (*4*). There have been numerous kinetic and spectroscopic studies on CODH/ACS and on ACS alone(*5*−*13*), yet there remain significant controversies over the mechanism of acetyl-CoA synthesis by ACS. For example, there has been significant discussion about what is the redox state of the active form of the enzyme both before and after binding CO (*14*, *15*).

In 1982, an unusual EPR signal was identified that is elicited when the enzyme is exposed to CO under reducing conditions (*16*). The observation of hyperfine splittings in the EPR spectrum when the CODH/ACS was isolated from *M. thermoacetica* cells that had been grown in the presence of ^{61}Ni, ^{57}Fe, and ^{13}CO helped to assign the metallocluster that elicits this spectrum as a novel NiFeS cluster (called the A-cluster) that binds CO; thus, the characteristic EPR signal became known as the NiFeC signal (also called A_{red}-CO or Ni^{1+}-CO) (*17*). A combination of crystallographic data and kinetic studies showed that the A-cluster contains a proximal metal ion (M_p), which is Ni in the active enzyme but Cu or Zn in the inhibited enzyme. This metal is called proximal due to its proximity to the [Fe_4S_4] cubane. Ni_p is bridged on one side through a cysteine residue to a [Fe_4S_4] cluster and on the other side to a square-planar distal Ni_d (*18*−*20*). Although it is clear that the A-cluster is the catalytic center that catalyzes the synthesis of acetyl-CoA from CO, the methylated CFeSP, and CoA (*14*, *15*, *21*), significant questions remain about the mechanism.

Scheme 1 outlines a mechanism, the so-called "paramagnetic mechanism", that involves paramagnetic intermediates. The major reason for supporting such a mechanism is that, when ACS

†This research was supported by grants to S.W.R. (NIH, GM-39451).
*To whom correspondence should be addressed. Tel: 734-615-4621. Fax: 734-763-4581. E-mail: sragsdal@umich.edu.

[1]Abbreviations: ACS, acetyl-CoA synthase; CODH, carbon monoxide dehydrogenase; CoA, coenzyme A; Fd, ferredoxin; Ni_p, proximal nickel in the binuclear site of the A-cluster of ACS; Ni_d, distal nickel in the binuclear site of the A-cluster of ACS; NiFeC, nickel−iron−carbon signal from the Ni^{1+}-CO intermediate; EPR, electron paramagnetic resonance; MV, methyl viologen.

 Published on Web 12/08/2010

Scheme 1: Proposed Paramagnetic Mechanism of ACS with Possible Fd-II Involvement[a]

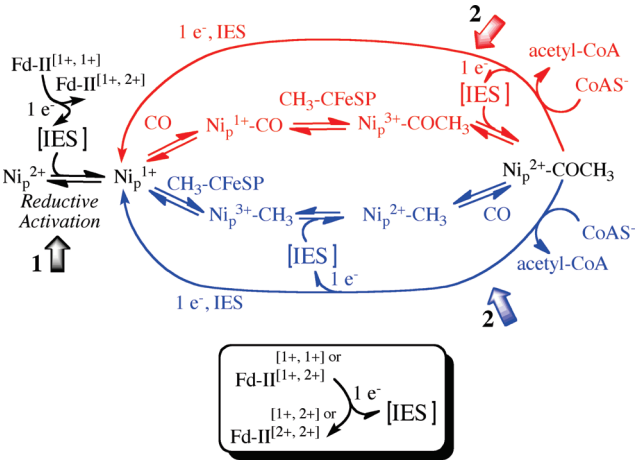

[a]This scheme depicts the random nature of the methylation and carbonylation steps of the ACS mechanism, with the "carbonylation-first" mechanism shown above in red and the "methylation-first" mechanism shown below in blue. The scheme also explicitly shows the internal electron shuttle (IES) that equilibrates electrons during reductive activation and at one stage of the catalytic cycle. The numbered block arrows depict the two stages of the ACS reaction studied in this paper. The lower panel shows the interaction of Fd-II with that IES.

is exposed to CO under reducing conditions, the EPR-active A_{red}-CO intermediate (described above) forms and decays (after reaction with the methylated CFeSP) at catalytically relevant rates (*5*, *13*, *22*). Because binding of CO is not a redox reaction, the first two steps in the mechanism were proposed to involve paramagnetic intermediates, e.g., Ni^{1+} and Ni^{1+}-CO. Recently, the Ni^{1+} intermediate to which CO binds was trapped and identified by photolysis and spectroscopic (EPR and infrared) studies (*23*). This Ni^{1+} species exhibits an EPR spectrum with *g*-values at 2.56, 2.10, and 2.01 and has an extremely low (1 kJ/mol) barrier for recombination with CO (*23*). Furthermore, stopped-flow infrared studies coupled with freeze−quench EPR experiments showed that reaction of ACS with CO generates the Ni^{1+}-CO intermediate and that this is the only carbonylated species that develops at catalytically competent rates (*22*). Thus, if carbonylation is the first step in the ACS mechanism, the involvement of Ni^{1+} and Ni^{1+}-CO as catalytic intermediates is well substantiated (i.e., the presence of a Ni^0-CO intermediate could be strictly ruled out).

However, one unsettling issue related to the so-called "paramagnetic" mechanism is that the reaction of ACS with the methylated CFeSP appears to occur through a nucleophilic attack of ACS on the methyl-Co^{3+} state of the CFeSP to generate Co^{1+} (*24*, *25*). Therefore, the S_N2 addition of a CH_3^+ group to Ni^{1+} or Ni^{1+}-CO would be expected to give a paramagnetic methyl-Ni^{3+} or acetyl-Ni^{3+} (or $[CH_3]$-Ni^{3+}-[CO]) state, respectively, as shown in Scheme 1. However, the product that is detected is EPR-silent and presumably diamagnetic (*12*, *13*, *26*). Thus, either the active species that reacts with the methyl group is diamagnetic, e.g., Ni^0, as suggested by the "diamagnetic" mechanism (*14*) (which would provide a straightforward explanation for the formation of a Ni^{2+} methylation product, methyl-Ni^{2+} or acetyl-Ni^{2+}), or the methylation is followed by a rapid one-electron uptake to reduce the methyl-Ni^{3+} or acetyl-Ni^{3+} intermediate to the related Ni^{2+} intermediate that is EPR-silent (*15*) (Scheme 1). Thus, the "diamagnetic" mechanism avoids the requirement for an as yet unidentified one-electron shuttle; however, it proposes (i) that the active catalyst is an even lower valence redox state of Ni (Ni^0 (*6*) or a spin-coupled species with Ni and the cluster in the 1+ states (*9*)) that has not been observed to have any catalytic relevance and (ii) that the Ni^{1+}-CO intermediate, whose catalytic competence has been demonstrated by various kinetic and spectroscopic methods (*13*, *27*), is an inhibited state (*28*). One of the goals of this paper is to address the involvement of a redox shuttle in the ACS mechanism.

Another issue that distinguishes the paramagnetic and diamagnetic ACS mechanisms is whether carbonylation or methylation of Ni_p occurs first. The diamagnetic mechanism strongly implies that methylation to form the EPR-silent Ni(II)-CH_3 state is the first step in acetyl-CoA synthesis. However, the paramagnetic mechanism, as depicted in Scheme 1, accommodates recent studies that indicate a random sequential mechanism (*3*), where formation of either Ni_p^{1+}-CO or Ni_p-CH_3 can be the first step. If the methylation and carbonylation steps in the ACS mechanism are random (*3*), the same Ni^{1+} catalyst that has been shown to form Ni^{1+}-CO (*23*) would be expected to be involved in the methylation reaction.

Thus, to summarize the catalytic cycle (Scheme 1) that we are testing in the current paper, the diamagnetic Ni^{2+} state of the proximal Ni center undergoes reductive activation to generate the active Ni^{1+} state. Then, in the "carbonylation-first" branch of the mechanism, CO binds to the Ni^{1+} species to form the paramagnetic A_{red}-CO (Ni^{1+}-CO) intermediate. Next, the methyl group binds to form an acetyl-Ni^{3+} intermediate, which is rapidly reduced through a one-electron shuttle to form an acetyl-Ni^{2+} species. Finally, CoA binds and serves as a nucleophile to release acetyl-CoA in a reaction that transfers one electron to the A-cluster of ACS to regenerate the active Ni^{1+} starting species and the other electron to the internal electron shuttle that can rereduce the acetyl-Ni^{3+} in the next round of catalysis. Possible internal mediators are the $[Fe_4S_4]$ subcluster and the distal Ni^{2+} center of the A-cluster, while external mediators include the $[Fe_4S_4]$ clusters of the CFeSP, one of the redox centers (the B- or D-clusters) in the CODH subunit, and ferredoxin (e.g., ferredoxin-II, Fd-II (*29*)), which had been isolated earlier as a cellular factor that stimulates acetyl-CoA synthesis (*30*). The experiments in this paper especially focus on the two steps of the catalytic cycle indicated by the two block arrows in Scheme 1, labeled as 1 and 2, and which refer to the initial reduction of the A-cluster, and the final acetyl-CoA synthesis steps, respectively. In the methylation-first branch of Scheme 1, the methyl group binds to the Ni_p^{1+} species to form the CH_3-Ni_p^{3+} state, which is followed by one-electron reduction to methyl-Ni_p^{2+}, followed by carbonylation to form acetyl-Ni^{2+} (this state is common to both mechanisms) and reaction with CoA to re-form the Ni_p^{1+} catalyst. When the methyl group binds first, it is the high valent CH_3-Ni_p^{3+} state that is reduced by the internal redox shuttle.

One of the goals of the experiments described in this report is to identify the redox state of the active form of ACS that participates in acetyl-CoA synthesis. We used controlled potential enzymology experiments to study the effect of redox potential on the rate of the CO/[1-^{14}C]-acetyl-CoA exchange reaction, which we will describe henceforth as the CO/acetyl-CoA exchange reaction (eq 1). In this ACS-catalyzed reaction, the radioactively labeled carbonyl group of [1-^{14}C]-acetyl-CoA undergoes isotopic exchange with ^{12}CO (*30*, *31*). This reaction has often been used in studies of CODH/ACS, because it involves all of the major steps of acetyl-CoA synthesis, i.e., the organometallic intermediates formed on ACS plus the C−C and C−S bond forming steps,

but is much less complicated, requiring only ACS as a catalyst. The controlled potential enzymology experiments identified a one-electron redox process with a midpoint potential that coincides with that for generation of the A_{red}-CO state of ACS. Another goal was to address the hypothesis that a one-electron shuttle is involved in acetyl-CoA synthesis by studying various reactions of the acetylated state of ACS. For example, the acetyl-Ni^{2+} state of ACS could reduce Fd-II by one electron, suggesting that there is a one-electron reservoir in this state of the enzyme. Furthermore, when CoA was added to acetyl-ACS in the presence of Fd-II and an excess of CO, one electron underwent transfer to the A-cluster to generate A_{red}-CO and the other electron was transferred to Fd-II. We also demonstrated that Fd-II can act as the electron donor for the reductive activation of ACS, as well as serving as an electron acceptor in the reaction of CoA with acetylated ACS at the end of the catalytic cycle. These combined results are in accord with the predictions of the "paramagnetic" mechanism of acetyl-CoA synthesis.

$$H_3C\text{-}^{14}CO\text{-}SCoA + CO \leftrightarrow H_3C\text{-}CO\text{-}SCoA + {}^{14}CO \quad (1)$$

MATERIALS AND METHODS

Purification of ACS and Fd-II. All growth and purification steps were done in glassware and plasticware that were washed with 3 M HCl and rinsed with Nanopure deionized water to eliminate the adventitious Cu^{2+} and Zn^{2+} that inhibit ACS. The *M. thermoacetica* ACS subunit was overexpressed in the *Escherichia coli* strain BL21(DE3)* from a pet29a(+) vector with a C-terminal His tag. The cells were grown, and ACS was overexpressed as described earlier (*3*). The cells were harvested, and ACS was purified using a Ni-NTA column (QIAGEN) in an anaerobic chamber (Vacuum Atmospheres, Inc.) under a N_2 atmosphere with O_2 concentration maintained below 1 ppm. Typically, cells from a 10 L culture were resuspended in 200 mL of lysis buffer, sonicated for 12 min, and ultracentrifuged at 30000 rpm for 50 min. After the column was loaded with cell extract, it was washed with 50 mM KP_i at pH 8.0 containing 300 mM NaCl, 2 mM β-mercaptoethanol, and 30 mM imidazole. ACS was eluted using the same buffer containing 90 mM imidazole. After elution, the most concentrated ACS fractions were pooled, and ACS was Ni-reconstituted in the elution buffer with 6 equiv of $NiCl_2$ for 2 or 3 days at 27 °C or at 45 °C. After Ni reconstitution, the protein was buffer exchanged into either 50 mM Tris (pH 7.6) or 50 mM KP_i (pH 7.5) with 20 mM KCl and 50−100 μM DTT. The NiFeC signal was quantitated by EPR to be somewhere between 0.3 and 0.8 spin/molecule depending on the purification and the conditions of Ni reconstitution.

Fd-II Was Purified from M. thermoacetica. The cells were grown anaerobically on 0.1 M glucose and 100% CO_2 (*32*) at 55 °C, and they were harvested when the OD at 600 nm reached ~5. The subsequent steps of the purification were done in the anaerobic chamber. The cell extract was applied to a 1 L DEAE-cellulose (Sigma-Aldrich) column, which was equilibrated with 50 mM Tris, pH 7.6, 2 mM dithionite, 2 mM dithiothreitol (DTT), and 0.1 mM methyl viologen (MV). The elution was done with a step gradient of increasing NaCl concentration, and Fd-II eluted at 0.5 M NaCl. The ferredoxin fraction was diluted to 0.15 M NaCl and applied to a Q-Sepharose (Sigma-Aldrich) column that was preequilibrated with 0.15 M NaCl. A salt gradient of 0.15−0.8 M NaCl was applied to the column, and Fd-II eluted at 0.65 M NaCl. The Fd-II fractions from the Q-Sepharose column were then purified further using a phenyl-Sepharose (GE Healthcare) hydrophobic interaction column, which was preequilibrated with the aforementioned Tris buffer at 90% $(NH_4)_2SO_4$ saturation. Fd-II and impurities were bound to the column at 90% $(NH_4)_2SO_4$. Then a gradient was run from 85% $(NH_4)_2SO_4$ saturation to 50% saturation, and Fd-II eluted out of the column at ~70% saturation. Fd-II was then concentrated and extensively buffer exchanged (5×, 1:15 dilution) into 50 mM Tris (pH 7.6) using Amicon Ultra centricons (Millipore) with 3 kDa molecular mass cutoff. The final purity and concentration were determined by SDS−PAGE (Supporting Information Figure S1) and UV−visible absorbance spectroscopy (Figure 1a). Immediately after purification, Fd-II was in the fully reduced state even though no chemical reductant was present in the final storage buffer, and it stayed in this state for about a few weeks in the anaerobic chamber. The amount of buffer exchange after purification, where the buffers contained 2 mM dithionite, 2 mM DTT, and 0.1 mM MV, would put the final concentrations in the storage buffer in the nanomolar range; therefore, it is highly unlikely that the residual dithionite concentrations in the purified Fd-II are high enough to interfere with experiments where Fd-II was used as a reductant. As described below, the UV−visible spectrum of Fd-II was also checked immediately before experiments to ensure the correct redox state for Fd-II, and if there were relatively high concentrations of redox reagents still present in solution, it would have been obvious in these spectra.

EPR and UV−Visible Spectroscopy and HPLC. EPR spectra were taken using a Bruker ESP300e spectrometer equipped with a ER 041 X microwave bridge, B-E 25 magnet, ER 083 C power source, 4119HS cavity, and an Oxford Instruments cryostat. UV−visible spectra were taken using a USB4000 Oceanoptics detector and DH-2000 light source that were connected via fiber-optic light guides to a cell holder in the anaerobic chamber. CoA and acetyl-CoA amounts in the reactions were quantitated after taking reaction aliquots quenched with 2.2 N perchloric acid (HOCl). After quenching, the aliquots were cleaned from precipitates by centrifugation and filtration. CoA and acetyl-CoA were separated on a C18 column (Luna 5u C18(2) from Phenomenex, Inc.) using a mobile phase of 20 mM acetate−tetramethylammonium hydroxide (pH 5.8) and a 0−20% acetonitrile gradient.

CO/[1-^{14}C]-Acetyl-CoA Exchange Assay. The CO/acetyl-CoA exchange assay was performed in 500 μL of 0.3 M MES buffer (pH 6.2) essentially as described in previous studies (*19*, *30*). The reaction mixture contained 200 μM [1-^{14}C]-acetyl-CoA and 20 mM KCl, and it was purged with 100% CO at 1 atm for 10 min. The reactions were initiated by the addition of 2−4 μM acetyl-CoA synthase, and 40 μL aliquots were taken out and quenched with 40 μL of 1 M HCl over the course of ~1 h. The quenched aliquots were mixed with EcoLume scintillation fluid (MP Biomedicals), and radioactivity was measured using a scintillation counter. The amount of radioactivity remaining in the reaction solution was plotted as a function of time and fit to an exponential decay function. The specific activities were calculated either from the exponential rates of the fits or the initial linear rates. When ACS was titrated with Fd-II to catalyze the CO/acetyl-CoA exchange activity, the following equation was used to fit the data:

$$v/V_{max} = [S]^n/(K_m + [S]^n) \quad (2)$$

where v is activity, V_{max} is maximum activity, [S] is substrate concentration, n is the number of binding sites, and K_m is an

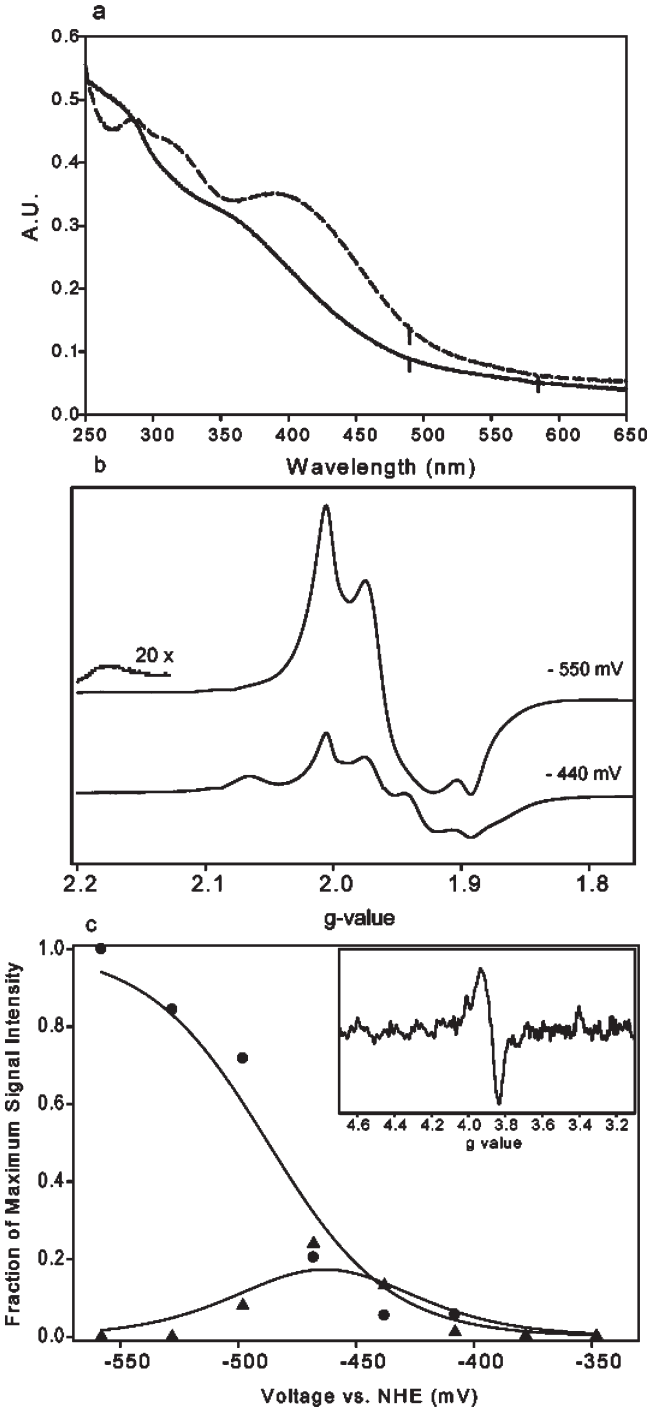

FIGURE 1: UV−visible, EPR, and electrochemical characterization of Fd-II. (a) UV−visible absorbance spectra of 11.2 μM Fd-II in 50 mM Tris (pH = 7.6) when it is reduced (solid line) versus oxidized (dashed line). (b) EPR spectra of Fd-II samples that were poised at representative potentials of −550 and −440 mV. The EPR parameters were as follows: frequency, 9.38 GHz; microwave power, 20 mW; receiver gain, 2000; modulation frequency, 100 kHz; modulation amplitude, 10.00 G. (c) Determination of the midpoint potential for Fd-II. The peak intensity vs potential plots for peaks at half-field ($\Delta m_s = 2$, $g = 3.88$, closed circles (●)) and at a g-value of 1.934 (▲), which were used to determine the fraction of each cluster at the reduced state. The fits were done using the equations described in Materials and Methods, and the redox potentials of −454 and −487 mV were determined for the two clusters. The half-field transition of the sample poised at −528 mV is shown in the inset.

apparent dissociation constant that is a function of the intrinsic dissociation constant and interaction factors (*33*).

Electrochemical Methods. An electrochemical cell was constructed as previously described (*34*, *35*). A 1 cm^2 gold plate connected to a 0.5 mm diameter gold wire was used as the working electrode, a 1 mm diameter silver wire was used as the counter electrode, and an Ag/AgCl electrode (Microelectrodes, Inc.) that had been calibrated against a calomel electrode (Bioanalytical Systems, Inc.) was used as a reference electrode. All electrochemical measurements and calibrations were done in the anaerobic chamber. The electrodes were connected to a CV-27 voltammograph from Bioanalytical Systems, Inc., and the electrochemical measurements were performed using the CV-27 voltammograph according to the manufacturer's instructions. To determine the midpoint potential of Fd-II, a 100 μM solution of Fd-II was poised at different voltages in the presence of 100 μM of each of the following electron mediators: 4,4′-dimethyl-2,2′-dipyridine, triquat, methyl viologen, and benzyl viologen. When the desired potential stabilized after 30−40 min, a sample was drawn out of the cell, transferred to an EPR tube, capped, and taken out of the chamber to be immediately frozen in liquid N_2. The following equations were used to fit the Nernst equation to the fractional signal intensities of the two $[Fe_4S_4]$ clusters (*36*, *37*):

$$R_A = [10^{(E-E_a)n/59}+1]^{-1} - [10^{(E-E_b)n/59}+1]^{-1} \quad (3)$$

$$R_B = [10^{(E-E_b)n/59}+1]^{-1} \quad (4)$$

In these equations, R_A represents the fraction of the primarily reduced cluster that gives rise to one set of EPR resonances, and R_B is the fraction of the secondarily reduced cluster that gives rise to another set of resonances. Analysis of the EPR data is explained in more detail in the Results section. E_a and E_b represent the midpoint redox potentials of the two clusters, E represents the solution redox potential in millivolts, and n is the number of electrons, which is 1 for each redox center. The signal intensity of the first cluster depends on the midpoint potentials of both clusters, as described by eq 3, because the signal from the first cluster increases as it undergoes reduction but then disappears as the second cluster is reduced. The signal from the doubly reduced state of Fd(II) is only seen as the second cluster gets reduced; therefore, the midpoint potential of the second cluster is obtained by fitting the intensity of this spectrum to eq 4.

When the CO/[1-^{14}C]-acetyl-CoA exchange was performed by controlled potential enzymology in the electrochemical cell, a solution containing 0.3 M MES buffer (pH 6.2), 200 μM [1-^{14}C]-acetyl-CoA, 20 mM KCl, and 100 μM of each electron mediator (triquat, 4,4′-dimethyl-2,2′-dipyridine, methyl viologen, and benzyl viologen) was purged with 100% CO in a separate vial, aliquots of this mixture were added to the electrochemical cell, and the gas phase above the solution was exchanged with CO. After 25−30 min, when the solution potential had stabilized, the exchange reaction was initiated by the addition of 20 μM ACS and monitored by removing aliquots for radioactivity measurements over a period of ~1 h at 27 °C. The plots of activity versus potential were fit to the following version of the Nernst equation (eq 5), where A_{obs} and A_{max} represent the observed and maximum specific activities, E represents the solution potential, E_m represents the midpoint potential of the redox active species, and n is the number of electrons. When data sets from different enzyme

preparations and experiments were combined, the activities were represented as a percentage of the maximum activity.

$$A_{obs} = A_{max}/(10^{(E-E_m)n/59} + 1) \quad (5)$$

Preparation of Methylcobinamide and Methylation of ACS. Methylated cobinamide was synthesized by incubating the following mixture at 27 °C for ~16 h: 1 mM aquocyanocobinamide, 3.5 mM titanium(III) citrate, and 20 μL of methyl iodide in 4 mL of 50 mM Tris-HCl (pH 7.6). The methylcobinamide was then purified using a 1 cm × 20 cm G-25 desalting column, and its concentration was determined by using an extinction coefficient of 11.1 mM^{-1} cm^{-1} at 462 nm (*38*). ^{14}C-Labeled methyl iodide (American Radiolabeled Chemicals, Inc.) was used to generate radioactive methylcobinamide. The methylation of ACS was performed by incubating 64 μM ACS with 2.5 equiv of methylcobinamide and 3 mM titanium(III) citrate at 45 °C for 2.5 h. The methylated ACS was then separated from methylcobinamide and titanium(III) citrate by performing buffer exchange 9−10 times using Amicon centrifuge filters with a 50 kDa molecular mass cutoff. Acetylated ACS was prepared by incubating the methylated ACS with 100% CO for 5 min. The protocol for the reaction of acetylated ACS with Fd-II and CoA is described in detail in the Results section.

RESULTS

Characterization of Fd-II by UV−Visible Spectroscopy and EPR. As shown in Figure 1a, the UV−visible spectrum of the purified *M. thermoacetica* Fd-II was very similar to that observed earlier (*29*), as well as for other 8Fe ferredoxins that contain two [Fe_4S_4] clusters (*39*−*42*). Since the purification buffers contained 2 mM dithionite, Fd-II was in the completely reduced form at the end of the purification protocol. Upon addition of 2 equiv of potassium ferricyanide, the intensity of the broad 390 nm peak increased, with a ratio of the absorbance values at 390 and 280 nm of ~0.75, which was indicative of pure protein in the oxidized state that is constituted with two clusters. Before each experiment, the redox state of Fd-II was determined by measuring its 390:280 absorbance ratio. This assessment of the Fd-II was especially important to ensure that external redox agents (e.g., dithionite and ferricyanide), after being used to poise the Fd-II at a suitable redox state for the experiment at hand, were removed from solution. The absorbance-based assay was typically done within 10 min before initiating an experiment and was useful in ensuring that the small molecule redox reagents, which also have visible absorbance spectra, were completely removed.

The EPR spectra of the different oxidation states of Fd-II were acquired at 13 K (Figure 1b) and were similar to those observed with other 2[Fe_4S_4] ferredoxins from anaerobic organisms (*43*, *44*). The sharp, organic radical EPR signals from the electron mediators are not very obvious in these spectra because they are present in stoichiometric amounts with respect to Fd-II (all at 100 μM) and because their EPR signals, unlike those of Fe-II, relax slowly and are saturated at low temperatures and high microwave powers (20 mW). The EPR spectrum of the two-electron-reduced form of Fd-II has a characteristic, complex line shape that results from the dipole−dipole and exchange interactions between the two $S = {}^1/_2$ clusters (*45*). In the fully reduced state, the main peaks are observed at *g*-values of 2.003, 1.960, and 1.892, and there are broader peaks at *g*-values of 2.173 and 1.762 (the $g = 2.173$ peak is shown at 20× magnification in Figure 1b). The EPR spectrum of the partially oxidized state contains peaks at *g*-values of 2.059 and 1.926 in addition to the peaks of the fully reduced state. These peaks are from a state of the enzyme that has only one reduced [Fe_4S_4] cluster. In Saeki et al., the EPR spectrum of a 2[Fe_4S_4] type ferredoxin from *Butyribacterium methyltrophicum* was analyzed by using individual peaks as signatures for different oxidation states of ferredoxin (*46*). In a similar fashion, we poised the redox potential of the solution at different values and froze aliquots of Fd-II for EPR analysis (Figure 1c). The peak at $g = 1.934$ was used as a signature peak to calculate the fraction of the reduced state of the cluster that has higher potential. The absolute spin concentration of this cluster was calculated by double integrating the whole EPR signal at −408 mV, where only the higher potential cluster is visible in the EPR spectrum. The fraction of the reduced cluster was extended to all other solution potentials by comparing the relative signal intensities of the $g = 1.934$ peak at different potentials. Since the peak at the half-field transition at $g = 3.88$ only forms when both clusters are reduced, it was used to calculate the fraction of the reduced state in the second cluster. The intensity of the half-field peak at the lowest potential is from the fully reduced second cluster, and the fractions of the reduced cluster in the rest of the potentials were calculated by using the relative half-field signal intensities. Finally, the curve for the first cluster was fit to the two-electron Nernst equation (eq 3), with E_a representing the midpoint potential for reduction of the first cluster and E_b representing that for reduction of the second cluster, which leads to disappearance of the representative $g = 1.934$ resonance of the first cluster. The curve for the second cluster was fit to the one-electron Nernst equation, since the appearance of the half-field signal depends on the reduction of the second cluster by one electron. The midpoint potentials (E_m values) for the two [Fe_4S_4] clusters were calculated to be -454 ± 10 and -487 ± 6 mV.

Activation and Reduction of ACS by Fd-II. Reduced Fd-II has a stimulatory effect on the CO/acetyl-CoA exchange reaction catalyzed by ACS (Figure 2a). Fitting of the activation curve to eq 2 gives a Hill coefficient of 2.2 ± 0.7 and an apparent K_m value of 36.9 ± 6.3 μM, indicating that ACS forms a fairly weak or transient interaction with Fd-II, as is often the case with electron transfer complexes. Our studies of the interaction between ACS and Fd-II complement earlier studies in which Fd-II was isolated as a factor that stimulates the CO/acetyl-CoA exchange reaction and was proposed to play a role in an internal electron transfer that occurs during the cleavage of the methyl and the CoA groups of acetyl-CoA (*30*). By cross-linking and mass spectrometric methods, an electrostatically stabilized complex between Fd-II and bifunctional CODH/ACS was mapped to a region defined by a peptide that includes residues 229−259 of the ACS subunit (*47*). The Hill coefficient indicates that the interaction between Fd-II and ACS is cooperative and implies that 2 mol of Fd-II may be involved in these interactions; however, stoichiometries are not reliable outputs of the Hill equation.

The activation of ACS was also observed by following the formation of the NiFeC signal after ACS is exposed to reduced Fd-II (Figure 2b). When ACS by itself was exposed to CO, no EPR signal was observed (top spectrum), whereas when ACS was preincubated with reduced Fd-II and then exposed to CO, the Ni^{1+}-CO intermediate formed (middle and bottom spectra). ACS was not exposed to any other reductant; however, Ti(III) or reduced methyl viologen can also chemically reduce ACS and induce formation of the Ni^{1+}-CO species. The intensity of the

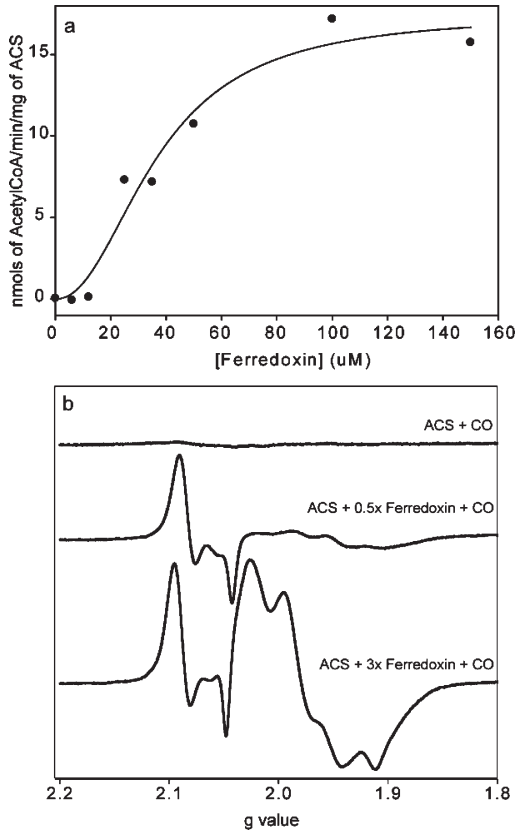

FIGURE 2: Reductive activation of ACS by Fd-II. (a) The increase in CO/acetyl-CoA exchange activity is shown as a function of Fd-II concentration. The assay was done at 55 °C with 4 μM ACS (30% NiFeC) in 0.3 M MES (pH = 6.2), 200 μM acetyl-CoA, 5 μM ^{14}C-labeled acetyl-CoA, and ~700 μM CO and titrated with different concentrations of Fd-II between 0 and 150 μM. The activation curve was fit with a Hill coefficient of 2.2 ± 0.7, and the apparent dissociation constant was estimated to be 36.9 ± 6.3 μM. (b) The reduction of ACS by Fd-II was monitored by measuring the formation of the NiFeC signal. The molar equivalencies of Fd-II were 0, 0.5, and 3. The EPR parameters were the same as in Figure 1 except that the microwave power here was 1 mW.

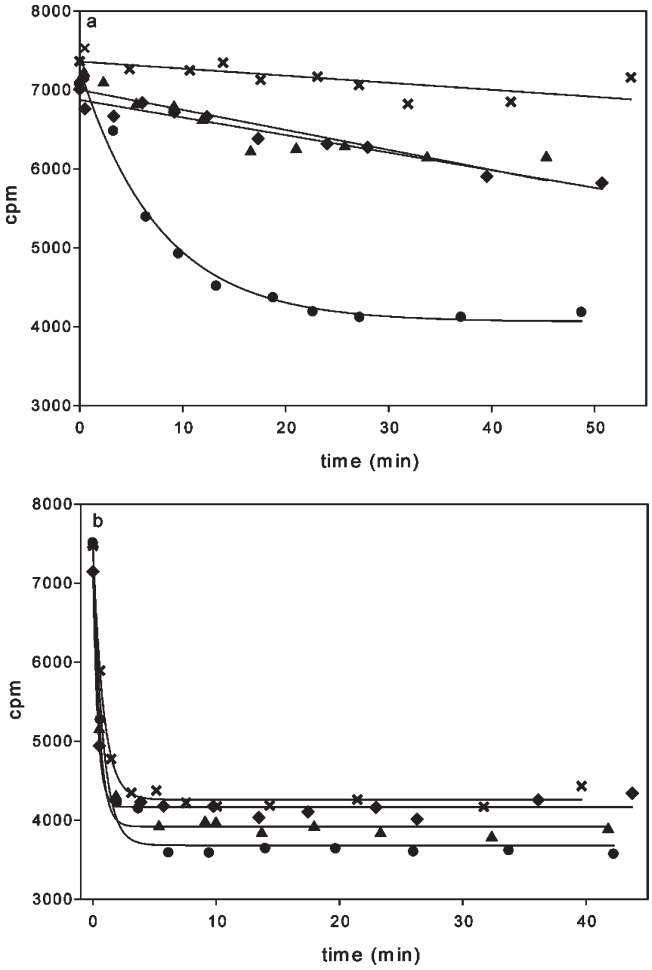

FIGURE 3: Effect of modulation of the redox states of Fd-II and ACS on ACS activity. The radioactive acetyl-CoA decay curves from CO/acetyl-CoA exchange assays at 55 °C using either unactivated ACS (a) or ACS prereduced by 10 mol equiv of dithionite (b). The different oxidation states of Fd-II are symbolized by (×) no Fd-II, (▲) partially oxidized Fd-II, (◆) oxidized Fd-II, and (●) reduced Fd-II. The concentration of ACS (50% NiFeC) was 4 μM in (a) and 1.8 μM in (b). The concentration of Fd-II was 30 μM in all reactions. All of the concentrations of other ingredients were the same as in the Figure 2 legend. The specific activities obtained from the reactions are summarized in Table 1.

NiFeC signal increased 1.4-fold as the Fd-II concentration was increased from 0.5 to 3 mol equiv of ACS.

The initial state of ACS in these assays is indicated by the first block arrow in Scheme 1. In contrast to the acetyl-CoA synthesis reaction shown in Scheme 1, the exchange reaction starts with the addition of acetyl-CoA to the reductively activated state of the enzyme, which leads to cleavage of the C−C and C−S bonds and formation of a quaternary complex in which the methyl, ^{14}CO, and CoA groups are bound to the A-cluster, followed by the exchange of ^{12}CO with the Ni-^{14}CO complex and re-formation of unlabeled acetyl-CoA and ^{14}CO. Although the CO/acetyl-CoA exchange reaction involves a few extra steps relative to the synthesis from bound precursors, it seems likely that reductive activation of ACS occurs similarly for the synthesis and exchange reactions.

Because the role of Fd-II in activation of ACS is presumably to perform a one-electron reduction of the Ni^{2+} center to the Ni^{1+} state, the effect of the oxidation state of Fd-II on activation of the CO/acetyl-CoA exchange reaction was determined (Figure 3a). The reduced, partially oxidized, and fully oxidized states of Fd-II were prepared by the incubation of as-isolated Fd-II with 2 mol equiv of dithionite, 0.5 equiv of potassium ferricyanide, or 2 equiv of potassium ferricyanide, respectively. After treatment, all oxidants and reductants were removed by centrifugal filtration. The oxidation state of Fd-II was determined by measuring the ratio of the absorbance values at 390 and 280 nm (A_{390}/A_{280}), which was 0.75 for oxidized Fd-II, 0.68 for partially oxidized Fd-II, and 0.6 for reduced Fd-II. As shown in Figure 3a and Table 1, with as-isolated ACS, incubation with reduced Fd-II provided the highest activity. When ACS was prereduced with dithionite (which was then removed by centrifugal filtration) before incubation with oxidized, partially reduced, or fully reduced Fd-II, the oxidation state of Fd-II does not have as extensive an effect on the rate of the reaction, and all activities

Table 1: Specific Activities for Figure 3 in μmol min^{-1} (mg of ACS)$^{-1}$

	as-isolated ACS	prereduced ACS
no Fd-II	0.0007 ± 0.0002	1.5 ± 0.1
reduced Fd-II	0.0790 ± 0.0086	1.5 ± 0.2
partially reduced Fd-II	0.0022 ± 0.0004	2.4 ± 0.2
oxidized Fd-II	0.0020 ± 0.0002	3.2 ± 0.3

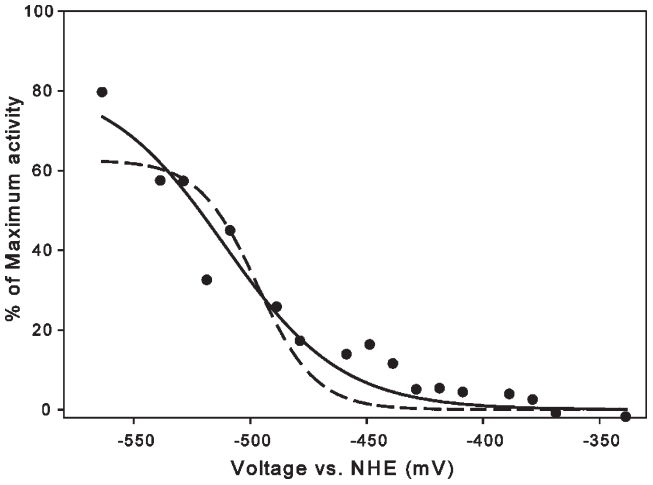

FIGURE 4: Dependence of ACS activity on solution redox potential. The specific activity of the CO/acetyl-CoA exchange reaction was measured at different solution potentials at 27 °C in an electrochemical cell in the anaerobic chamber. The buffer and the concentrations of different ingredients were the same as in the Figure 2 legend, except for ACS, which was 20 μM. In addition, 100 μM each of the following redox mediators was included: 4,4′-dimethyl-2,2′-dipyridyl, methyl viologen, benzyl viologen, and triquat. The trend in specific activity was plotted using either the one-electron (solid line) or the two-electron (dashed line) Nernst equation. The R^2 value for the one-electron fit is 0.9437, whereas for the two electron fit, it is 0.8583. The midpoint redox potential according to the one-electron Nernst equation is -511 ± 6 mV.

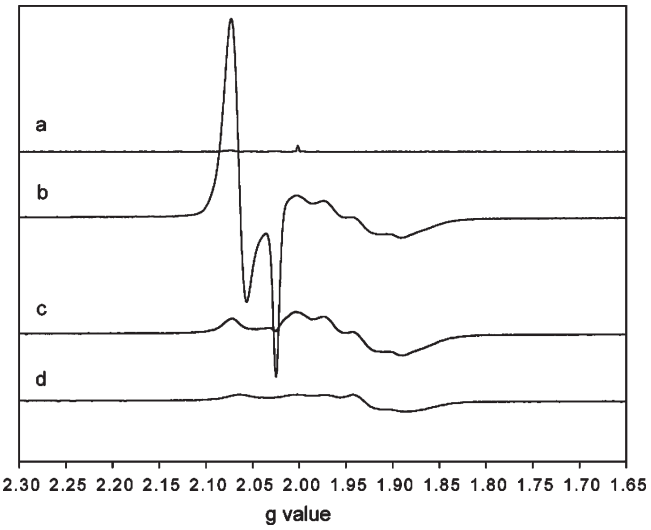

FIGURE 5: Measurement of electron transfer from acetylated ACS to Fd-II. The acetylated ACS sample was reacted with CoA in the presence of oxidized Fd-II (b). Also shown are the EPR spectra of acetylated ACS (a), acetylated ACS incubated with Fd-II without any CoA (c), and oxidized Fd-II by itself (d). All of the reactions were performed in 50 mM KP_i buffer (pH 7.5) and 20 mM KCl. The ACS, Fd-II, and CoA concentrations were 69, 100, and 500 μM, respectively. The EPR spectra were taken at 10 K, and the parameters were as follows: frequency, 9.38 GHz; microwave power, 10 μW; receiver gain, 50000; modulation frequency, 100 kHz; modulation amplitude, 10 G.

are considerably higher than when ACS is not prereduced (Figure 3b). Table 1 also summarizes the activities observed using different oxidation states of ACS and Fd-II. When ACS is prereduced by dithionite, much higher activities are observed in general than when ACS is not prereduced. However, when ACS is not prereduced, the highest activity is observed when Fd-II is reduced, which suggests that activation by Fd-II observed in Figure 2 is due to a reduction event.

Reductive Activation of CO/Acetyl-CoA Exchange Activity in the Electrochemical Cell. The effect of the redox potential on the CO/acetyl-CoA exchange activity was studied by performing the exchange assay in an electrochemical cell with electron mediators (Figure 4), as described in the Materials and Methods section. The CO/acetyl-CoA exchange reaction is itself not a redox reaction, so the exchange rate should follow a Nernst curve that reflects the midpoint potential for the inactive/active catalyst and the number of electrons required for activation. The rate of exchange increased as the solution potential was lowered. Although it was not possible to poise the solution potential at voltages lower than ~ -560 mV in the electrochemical cell, we adequately fit the data to a Nernst equation (eq 5) with a significantly better fit to a one-electron as opposed to a two-electron reduction, as shown by the solid and dotted lines in Figure 4. The standard deviations and goodness of fit parameters were significantly better for the one- versus the two-electron fit. From this analysis, the midpoint redox potential of the form of ACS undergoing reductive activation by one electron was -511 ± 6 mV (*5*).

Reaction of Acetylated ACS with CoA and Fd-II. The step of the catalytic cycle in which the acetylated ACS reacts with CoA to form acetyl-CoA is shown with the second block arrow in Scheme 1. Studying this latter part of the ACS catalytic cycle makes it possible to follow the destination of the electrons that are released upon the nucleophilic attack of the thiol group of CoA on the acetyl-Ni(II) intermediate. We used EPR spectroscopy to follow electron flow to Fd-II and to ACS. Excess CO (below) was present to trap any ACS that had undergone reductive activation, and we note that CO does not act as a reductant of ACS. Also, as described below, two electrons are released as the acetyl-CoA is formed, and they separate with one electron ultimately ending up in Fd-II and the other electron being retained by the active site as indicated by the formation of the NiFeC signal.

To form the acetylated state, ACS was reacted with methylcobinamide, which was ^{14}C-labeled on the methyl group and then purged with 100% CO. The amount of radioactivity on ACS after it was methylated indicated that there were 2.2 methyl groups per ACS monomer. It is surprising that more than a stoichiometric number of methyl groups are found per ACS monomer according to quantitation of radioactivity on ACS after methylation. This is possibly due to the long duration of the methylation reaction with a non-native methylating agent (i.e., methylcobinamide instead of CFeSP) and a nonspecific methyl group transfer to a nucleophilic methyl acceptor in the active site or somewhere else on the protein. After methylation of ACS, the reacted cobinamide and unreacted methylcobinamide were removed by extensive buffer exchange. Since there are not any methyl group donors other than ACS in the final reaction mixture with acetylated ACS, the reaction takes place under single-turnover conditions.

The reaction of acetylated ACS (69 μM) with oxidized Fd-II (100 μM) and CoA (500 μM) was studied by EPR spectroscopy and by measuring the amount of acetyl-CoA that is synthesized during the final step of the cycle. All reactions were performed in 50 mM KP_i (pH = 7.5) and 20 mM KCl at 55 °C for $\sim$6 min under 1 atm of CO. In the first control reaction, which is shown in Figure 5a, buffer was added to the acetylated ACS instead of Fd-II or CoA, and the spectrum shows that acetylated ACS remained

Table 2: Quantitation of Electrons Released during the Final Step of Acetyl-CoA Synthesis

	NiFeC, μM (spins/ACS)[a]	Fd(II) reduced, μM (fraction of ACS)[a]	acetyl-CoA formed, μM (fraction of ACS)[a]	released electrons, μM (fraction of ACS)[a]	(NiFeC + Fd-II reduced) − released electrons, μM (fraction of ACS)[a]
ACS + Fd(II) + CoA, reaction 1	48 (0.7)	35 (0.51)	40 (0.58)	80 (1.16)	3.4 (0.05)
ACS + Fd(II) + CoA, reaction 2	44 (0.64)	42 (0.61)	53 (0.77)	106 (1.54)	−20 (−0.28)
ACS + Fd(II) + CoA, reaction 3	49 (0.71)	36 (0.52)	53 (0.77)	106 (1.54)	−21 (−0.3)
ACS + Fd(II)	1.4 (0.02)	45 (0.65)			
ACS + CoA, reaction 1	40 (0.57)		32 (0.46)	64 (0.92)	−24 (−0.35)
ACS + CoA, reaction 2	36 (0.53)		56 (0.81)	112 (1.62)	−76 (−1.1)
ACS + CoA, reaction 3	39 (0.57)		59 (0.86)	118 (1.72)	−79 (−1.14)

[a]The value in μM is followed by the fractional value relative to the concentration of ACS.

EPR silent. When acetyl-ACS was reacted with oxidized Fd-II and CoA (b), an intense EPR signal between $g = 2.02$ and 2.08 was observed, which is the characteristic spectrum of the NiFeC species of ACS. The reaction of acetyl-ACS with Fd-II and CoA was performed in triplicate, and the results are summarized in Table 2. The average amount of the NiFeC intermediate that accumulated after addition of CoA/Fd-II in three reactions was 0.68 spin/mol of ACS, as determined by the double integration of the NiFeC signals at 70 K. Based on HPLC quantitation, the amount of acetyl-CoA formed in the reaction corresponded to 0.71 equiv of ACS. Besides the NiFeC signal, the spectrum of reduced Fd-II, comprised of the broader peaks centered around $g = 1.94$ and amounting to 0.79 spin/mol of Fd, appeared after the reaction with CoA. Before reacting with ACS (Figure 5d), the EPR signal of Fd-II amounted to a spin concentration of 0.47 spin/mol of Fd-II. Subtraction of the EPR spectra of reduced Fd-II after versus before addition of CoA showed that it received an amount of electrons that corresponded to an average of 0.55 equiv of ACS. The finding that 0.71 equiv of acetyl-CoA releases electrons to reduce similar amounts of Ni_p and Fd-II indicates that the 2 reducing equiv released/mol of acetyl-CoA formed are roughly equally distributed between the ACS active site to re-form the NiFeC intermediate and the external electron acceptor, Fd-II. The average difference between the electrons expected to be released by acetyl-CoA synthesis (column 9 of Table 2) and the electrons accounted for by the NiFeC and Fd-II signals (columns 2 and 4 of Table 2) corresponds to 0.18 equiv of ACS (last column of Table 2).

As another control, ACS was incubated with Fd-II in the absence of CoA (Figure 5c). While this reaction did not yield acetyl-CoA, based on the quantitation of the EPR signal of Fd-II, acetylated ACS appears to be able to reduce Fd-II, with an amount of electrons corresponding to an average of 0.86 equiv of ACS even in the absence of CoA. During this reaction, only a small amount of NiFeC signal is formed, corresponding to 0.02 equiv of ACS, and no other paramagnetic intermediates were observed after electron transfer from an EPR-silent acetyl-ACS to Fd-II.

Acetylated ACS was also reacted with CoA in the absence of Fd-II in three identical reactions, the EPR spectrum of which is not shown, and the average yields of acetyl-CoA and the NiFeC signal in these reactions are 0.71 and 0.56 equiv of ACS, respectively, with an average of 0.86 equiv of electrons (per mole of ACS) released by acetyl-CoA formation that are unaccounted for. Thus, there appears to be a one-electron reservoir in the acetyl-ACS state that has a low enough redox potential to reduce Fd-II.

DISCUSSION

ACS catalyzes the synthesis of acetyl-CoA through a series of enzyme-bound organometallic intermediates that are bound to the A-cluster. Based on the results of X-ray crystallographic (*18*, *20*), spectroscopic (EPR (*48*), Mössbauer (*49*, *50*), electron nuclear double resonance (ENDOR) (*17*), Fourier transform infrared (FTIR) (*22*, *51*)), biochemical (*19*, *52*, *53*), and computational (*54*) studies, the A-cluster is composed of a $[Fe_4S_4]$ cluster bridged through cysteine to the proximal Ni (Ni_p) of a dinuclear Ni center. Catalysis seems to occur at this Ni_p site, which changes ligation and oxidation states during catalysis, whereas the distal Ni (Ni_d), which is ligated by two deprotonated amides and two cysteine thiolates in a Cys-Gly-Cys motif, appears to remain square planar in the 2+ oxidation state.

A paramagnetic NiFeC (Ni_p^{1+}-CO) species is proposed to be an intermediate in the ACS mechanism because, among other reasons, it forms (after treatment with CO) and decays (after reaction with the methylated CFeSP) faster than the overall steady-state rate of acetyl-CoA formation (*5*, *13*, *22*) and because the NiFeC species is the sole metal−carbonyl species formed upon reaction of ACS with CO (*22*). At temperatures below 20 K, photolysis of the Ni_p^{1+}-CO species leads to the formation of what appears to be the Ni_p^{1+} species to which CO or the methyl group binds (*23*). The *g*-values of the novel Ni_p^{1+} state (2.558, 2.1, and 2.01) indicated that the unpaired electron is almost wholly localized on Ni_p. Because this species is so unstable and has not been observed in previous redox titrations, yet rapidly recombines with CO to generate Ni_p^{1+}-CO, it was proposed that initiation of the catalytic cycle (as shown in Scheme 1) involves a coupled reaction in which reductive activation of a diamagnetic inactive Ni_p^{2+} state to generate this very low potential Ni_p^{1+} center is coupled to carbonylation (to form Ni_p^{1+}-CO) or methylation (to form initially methyl-Ni_p^{3+}) (*23*).

We obtained further insight into the ACS mechanism by measuring the rate of the ACS-catalyzed CO/acetyl-CoA exchange reaction at different ambient solution redox potentials. Controlled potential enzymology experiments with the bifunctional CODH/ACS in the presence of CO are not feasible because CO reacts with CODH in the electrochemical cell and generates a catalytic current that dominates the electrochemistry. Having a highly active form of recombinant ACS (in the absence of CODH) allows control of the potential during the CO/acetyl-CoA exchange reaction. It was determined that a single electron at a midpoint redox potential of −511 mV is transferred during the activation of the A-cluster. This value is between the midpoint redox potential of −541 mV that was determined by Gorst et al. for formation of the NiFeC species from acetyl-CoA (*5*) and the

midpoint potential (−486 mV) measured for an isotopic exchange reaction between ^{14}C-CoA and acetyl-CoA (*55*). The same midpoint potential and one-electron activation was measured for the CoA/acetyl-CoA exchange reaction catalyzed by the ACS component of the methanogenic acetyl-CoA decarbonylase synthase (*56*). Because the initial state of the A-cluster has the cluster, Ni_p, and Ni_d in the 2+ states, these electrochemical results suggest that the activation of ACS involves the reduction of Ni^{2+} to Ni^{1+}. The combined experiments provide further evidence supporting the paramagnetic mechanism with the Ni_p^{1+}-CO intermediate as a catalytically competent intermediate.

Here we have studied the redox chemistry and the involvement of Fd-II in an internal electron transfer reaction during acetyl-CoA synthesis by ACS. Such a function was proposed over 25 years ago (*30*) when it was shown that, although the CODH/ACS-catalyzed CO/acetyl-CoA exchange reaction is not a net redox reaction, Fd-II markedly enhances the exchange rate, exhibiting a K_{act} value of 0.43 μM. The ACS interaction with Fd-II appears to be specific because, in these earlier studies, Fd-II was isolated from cell extracts as a factor that stimulates the CO/acetyl-CoA exchange reaction (*30*). Furthermore, by cross-linking, proteolysis, and mass spectrometric methods, an electrostatically stabilized complex between Fd-II and bifunctional CODH/ACS was mapped to a region defined by a peptide that includes residues 229−259 of the ACS subunit (*47*). Here we studied the interactions between ACS and Fd-II in the CO/acetyl-CoA exchange reaction and during a partial reaction in acetyl-CoA synthesis: the CoA-dependent cleavage of acetyl-ACS to form acetyl-CoA. When this exchange reaction is performed by the ACS subunit alone (i.e., lacking CODH), Fd-II acts as a reductive activator of ACS and possibly as an electron mediator during the catalytic cycle. Furthermore, the specific activity depends on the midpoint potential of the electron donor. When Fd-II was used as a reductant, the specific activity was 0.079 unit/mg. The midpoint potentials of the two $[Fe_4S_4]$ clusters of Fd-II are 24 and 57 mV more positive than that of the redox-active species in ACS, which makes this electron transfer thermodynamically unfavorable, and it may explain the slower exchange rates observed when Fd-II is used as a reductant instead of titanium(III) citrate. Furthermore, the apparent K_m of 37 μM observed with Fd-II and ACS in the exchange is ~85-fold higher than the K_m of 0.43 μM that was reported for Fd-II with the bifunctional CODH/ACS (*30*), which may be due to weaker binding between Fd-II and ACS when CODH subunit is absent. On the other hand, a specific activity of 0.72 unit/mg was reported when titanium(III) citrate (with a midpoint redox potential of −480 mV at pH 7 (*57*)) was the reductant (*3*). Furthermore, ~15-fold faster rates were observed when ACS was prereduced with dithionite than when ACS was exclusively activated by Fd-II; however, at higher concentrations, dithionite also acts as an inhibitor of the CO/acetyl-CoA exchange activity of the bifunctional CODH/ACS (*30*).

We also used Fd-II to follow the transfer of electrons during the reaction of CoA with acetyl-ACS, which represents the final step of acetyl-CoA synthesis. CoA acts as a nucleophile in this reaction and, as shown in Scheme 1, donates two electrons, one of which regenerates the active form of ACS, while the other reduces the Fd-II. Fd-II is not required for this reaction; in fact, similar amounts of acetyl-CoA are formed (0.71 equiv) in the absence of Fd-II. Fd-II also accepts electrons from acetylated ACS even in the absence of CoA (Figure 5c, Table 2, row 4), indicating that there is a site on acetyl-ACS, i.e., a "shuttle", from which electrons can be spontaneously transferred to Fd-II even though no observable EPR signal is observed from ACS before or after the electron transfer. That the electron transfer to Fd-II occurs in the absence of CoA is surprising; however, it is important to determine the rate constant for this electron transfer to determine if it is catalytically relevant. For example, in pyruvate ferredoxin oxidoreductase, CoA stimulates the rate of an internal electron transfer from a radical intermediate to an iron−sulfur cluster by 10^5-fold (*58*). There also is not a new EPR signal observed in reactions without Fd-II, even though an average of 0.86 ACS equiv of electrons are released in addition to the formation of the Ni^{1+}-CO intermediate (Table 2, final column, last three rows). The lack of an observable EPR signal on ACS associated with the "shuttle", which is apparently playing a role in both electron transfer from acetylated ACS to Fd-II and when acetyl-CoA is formed in the absence of Fd-II, points toward the complicated spin and magnetic properties of this internal "shuttle" and the active site. In reactions with and without Fd-II, a significant amount of the Ni^{1+}-CO intermediate is formed after the acetyl-CoA is made, corresponding to the averages of 0.68 and 0.56 equiv of ACS, respectively. This result indicates the presence of an electron shuttle in ACS that allows a significant portion (close to half) of the electrons that are generated during CoA-dependent cleavage of the acetyl−Ni bond stay at the Ni_p center and form the Ni^{1+}-CO intermediate when CO is present in the active site. This may represent a mechanism for conserving the electron necessary for the initial activation of the A-cluster, because it never leaves the active site to return the Ni_p to the original 2+ state. The other half of the electrons is released to the external reductant, Fd-II, if it is present. The destination of the released electrons, when Fd-II is not present, is unknown since there are not any observable EPR signals before or after electron transfer. We ruled out the possible loss of electrons by H_2 evolution due to proton reduction because we did not detect any H_2 formation during CoA-dependent acetyl-CoA formation from acetyl-ACS (data not shown). Because the acceptor must be a component of ACS, possible candidates for this electron shuttle include an EPR-silent state of the $[Fe_4S_4]$ portion of the A-cluster or a sulfur-based radical that is not observed by EPR due to broad resonances or exchange coupling to another paramagnet.

Our results concur with those of Gencic et al. (*59*), who showed that after CoA addition to the acetylated subunit β of the ACDS complex of *Methanosarcina thermophila*, 2 mol of methyl viologen (MV) was reduced/mol of acetyl-CoA formed. However, there was no information about whether the Ni^{1+}-CO intermediate is formed or what is the electronic state of Ni_p during or after the reaction (*59*). As shown in Figure 5, if CO is present in the active site, as was the case in the current study, one of the released electrons is sequestered by Ni_p to form the Ni^{1+}-CO intermediate. The redox potential of MV is also less negative than that of Fd-II, which gives a greater energy incentive to pass both electrons released during acetyl-CoA formation to MV.

Several recent studies on the ACS mechanism have been interpreted according to the diamagnetic mechanism (*6*, *9*, *60*); however, the major experimental support for the diamagnetic mechanism is that the methylated and acetylated states of the enzyme are "EPR-silent" and the methyl-Ni^{3+} state has not been observed (*61*). The inability to have trapped a methyl-Ni(III) catalytic intermediate is indeed a limitation of the paramagnetic mechanism; however, the diamagnetic mechanism suffers from a similar limitation in proposing the A-cluster to be in a rather unstable two-electron-reduced state (*6*, *9*, *14*) involving a net Ni^0

state that has not been observed and is unprecedented in biological systems. The midpoint redox potential of the $Ni^{2+/1+}$-CO couple is already lower than −550 mV; therefore, two-electron reduction of the Ni^{2+} (especially in the absence of the stabilizing effect of bound CO) will be extremely difficult. Furthermore, the stability of such a two-electron-reduced species is suspect in a highly electropositive environment with two other redox centers, Ni_d^{2+} and $[Fe_4S_4]^{2+}$ with much higher redox potentials adjacent to the hypothetical Ni_p^0. On the other hand, the Ni^{1+}-CO intermediate in the paramagnetic mechanism (that was proposed to be an inhibited state of the enzyme according to the diamagnetic mechanism) has been shown to be catalytically competent in acetyl-CoA synthesis, as described above. Furthermore, as shown in Scheme 1, the paramagnetic mechanism accommodates these EPR-silent methyl-Ni and acetyl-Ni states by including an internal redox shuttle that rapidly reduces methyl-Ni(III) to the methyl-Ni(II) state.

Bramlett et al. (*6*) showed that when methylated ACS is reacted with CO and CoA (in the presence of methylated corrinoid protein and in solutions that are devoid of reductant), acetyl-CoA is catalytically synthesized. The authors concluded that this experiment eliminates the paramagnetic mechanism as a viable possibility; however, this conclusion does not seem justified. The nucleophilic attack of $CoAS^-$ on methyl-ACS (and CO) adds two electrons into the system, which is fully consistent with the paramagnetic mechanism, as shown in Scheme 1. Because acetyl-CoA synthesis is not a net redox reaction, the addition of two electrons during the reaction of $CoAS^-$ with the acetyl-ACS intermediate supports continued catalysis regardless of whether the reaction occurs through a paramagnetic or diamagnetic mechanism. The only difference is whether one begins (and ends) with a diamagnetic or paramagnetic system.

In this paper, we show that Fd-II can act as a redox mediator by accepting electrons from the acetyl-ACS intermediate and by serving as the initial reducing agent linked to formation of the Ni^{1+}-CO catalytic intermediate. Both the reductive activation and electron shuttle roles would account for the as yet unexplained stimulation by Fd-II of the CO/acetyl-CoA exchange reaction that was observed 25 years ago (*30*). In its catalytic (electron shuttle) role, Fd-II interfaces with an unidentified internal redox shuttle in ACS (perhaps within the A-cluster itself), accepting an electron generated during the thiolytic cleavage of the acetyl-ACS intermediate and donating it back through the shuttle to reduce the proposed unstable high-valent methyl- or acetyl-Ni(III) species. It is important to identify the proposed internal redox shuttle that appears to mediate electron transfer to and from Fd-II.

SUPPORTING INFORMATION AVAILABLE

Figure S1 showing the SDS−PAGE analysis of purified Fd-II and Table S1 showing the same set of reactions as in Table 2 but performed separately on an earlier date. This material is available free of charge via the Internet at http://pubs.acs.org.

REFERENCES

1. Ragsdale, S. W., and Pierce, E. (2008) Acetogenesis and the Wood-Ljungdahl pathway of CO2 fixation. *Biochim. Biophys. Acta 1784*, 1873–1898.
2. Drake, H. L., Daniel, S. L., Kusel, K., Matthies, C., Kuhner, C., and Braus-Stromeyer, S. (1997) Acetogenic bacteria: what are the in situ consequences of their diverse metabolic versatilities? *BioFactors 6*, 13–24.
3. Seravalli, J., and Ragsdale, S. W. (2008) Pulse-chase studies of the synthesis of acetyl-CoA by carbon monoxide dehydrogenase/acetyl-CoA synthase—Evidence for a random mechanism of methyl and carbonyl addition. *J. Biol. Chem. 283*, 8384–8394.
4. Loke, H. K., Tan, X. S., and Lindahl, P. A. (2002) Genetic construction of truncated and chimeric metalloproteins derived from the alpha subunit of acetyl-CoA synthase from *Clostridium thermoaceticum*. *J. Am. Chem. Soc. 124*, 8667–8672.
5. Gorst, C. M., and Ragsdale, S. W. (1991) Characterization of the NiFeCO complex of carbon-monoxide dehydrogenase as a catalytically competent intermediate in the pathway of acetyl-coenzyme-A synthesis. *J. Biol. Chem. 266*, 20687–20693.
6. Bramlett, M. R., Stubna, A., Tan, X. S., Surovtsev, I. V., Munck, E., and Lindahl, P. A. (2006) Mossbauer and EPR study of recombinant acetyl-CoA synthase from *Moorella thermoacetica*. *Biochemistry 45*, 8674–8685.
7. Maynard, E. L., Tan, X., and Lindahl, P. A. (2004) Autocatalytic activation of acetyl-CoA synthase. *J. Biol. Inorg. Chem. 9*, 316–322.
8. Tan, X. S., Sewell, C., Yang, Q. W., and Lindahl, P. A. (2003) Reduction and methyl transfer kinetics of the alpha subunit from acetyl coenzyme A synthase. *J. Am. Chem. Soc. 125*, 318–319.
9. Tan, X., Martinho, M., Stubna, A., Lindahl, P. A., and Munck, E. (2008) Mossbauer evidence for an exchange-coupled {$[Fe_4S_4](1+)$ Ni-p(1+)} A-cluster in isolated alpha subunits of acetyl-coenzyme a synthase/carbon monoxide dehydrogenase. *J. Am. Chem. Soc. 130*, 6712–6713.
10. Tan, X. S., Surovtsev, I. V., and Lindahl, P. A. (2006) Kinetics of CO insertion and acetyl group transfer steps, and a model of the acetyl-CoA synthase catalytic mechanism. *J. Am. Chem. Soc. 128*, 12331–12338.
11. Tan, X. S., Sewell, C., and Lindahl, P. A. (2002) Stopped-flow kinetics of methyl group transfer between the corrinoid-iron-sulfur protein and acetyl-coenzyme A synthase form *Clostridium thermoaceticum*. *J. Am. Chem. Soc. 124*, 6277–6284.
12. Barondeau, D. P., and Lindahl, P. A. (1997) Methylation of carbon monoxide dehydrogenase from *Clostridium thermoaceticum* and mechanism of acetyl coenzyme A synthesis. *J. Am. Chem. Soc. 119*, 3959–3970.
13. Seravalli, J., Kumar, M., and Ragsdale, S. W. (2002) Rapid kinetic studies of acetyl-CoA synthesis: evidence supporting the catalytic intermediacy of a paramagnetic NiFeC species in the autotrophic Wood-Ljungdahl pathway. *Biochemistry 41*, 1807–1819.
14. Lindahl, P. A. (2004) Acetyl-coenzyme A synthase: the case for a Ni-p(0)-based mechanism of catalysis. *J. Biol. Inorg. Chem. 9*, 516–524.
15. Ragsdale, S. W. (2007) Nickel and the carbon cycle. *J. Inorg. Biochem. 101*, 1657–1666.
16. Ragsdale, S. W., Ljungdahl, L. G., and Dervartanian, D. V. (1982) Electron-paramagnetic-res evidence for nickel-substrate interaction in carbon-monoxide dehydrogenase from *Clostridium thermoaceticum*. *Biochem. Biophys. Res. Commun. 108*, 658–663.
17. Fan, C. L., Gorst, C. M., Ragsdale, S. W., and Hoffman, B. M. (1991) Characterization of the Ni-Fe-C complex formed by reaction of carbon-monoxide with the carbon-monoxide dehydrogenase from *Clostridium thermoaceticum* by Q-band ENDOR. *Biochemistry 30*, 431–435.
18. Doukov, T. I., Iverson, T. M., Seravalli, J., Ragsdale, S. W., and Drennan, C. L. (2002) A Ni-Fe-Cu center in a bifunctional carbon monoxide dehydrogenase/acetyl-CoA synthase. *Science 298*, 567–572.
19. Seravalli, J., Xiao, Y., Gu, W., Cramer, S. P., Antholine, W. E., Krymov, V., Gerfen, G. J., and Ragsdale, S. W. (2004) Evidence that NiNi acetyl-CoA synthase is active and that the CuNi enzyme is not. *Biochemistry 43*, 3944–3955.
20. Darnault, C., Volbeda, A., Kim, E. J., Legrand, P., Vernede, X., Lindahl, P. A., and Fontecilla-Camps, J. C. (2003) Ni-Zn-[Fe(4)-S(4)] and Ni-Ni-[Fe(4)-S(4)] clusters in closed and open alpha subunits of acetyl-CoA synthase/carbon monoxide dehydrogenase. *Nat. Struct. Biol. 10*, 271–279.
21. Drennan, C. L., Doukov, T. I., and Ragsdale, S. W. (2004) The metalloclusters of carbon monoxide dehydrogenase/acetyl-CoA synthase: a story in pictures. *J. Biol. Inorg. Chem. 9*, 511–515.
22. George, S. J., Seravalli, J., and Ragsdale, S. W. (2005) EPR and infrared spectroscopic evidence that a kinetically competent paramagnetic intermediate is formed when acetyl-coenzyme A synthase reacts with CO. *J. Am. Chem. So.c 127*, 13500–13501.
23. Bender, G., Stich, T. A., Yan, L., Britt, R. D., Cramer, S. P., and Ragsdale, S. W. (2010) Probing the catalytic mechanism of acetyl-CoA synthase by infrared and EPR characterization of the photolyzed Ni(I)-CO intermediate. *Biochemistry 49*, 7516–7523.

24. Menon, S., and Ragsdale, S. W. (1998) Role of the [4Fe-4S] cluster in reductive activation of the cobalt center of the corrinoid iron-sulfur protein from *Clostridium thermoaceticum* during acetyl-CoA synthesis. *Biochemistry 37*, 5689–5698.
25. Menon, S., and Ragsdale, S. W. (1999) The role of an iron-sulfur cluster in an enzymatic methylation reaction: methylation of CO dehydrogenase/acetyl-CoA synthase by the methylated corrinoid iron-sulfur protein. *J. Biol. Chem. 274*, 11513–11518.
26. Grahame, D. A., Khangulov, S., and Demoll, E. (1996) Reactivity of a paramagnetic enzyme-CO adduct in acetyl-CoA synthesis and cleavage. *Biochemistry 35*, 593–600.
27. Gorst, C. M., and Ragsdale, S. W. (1991) Characterization of the NiFeCO complex of carbon-monoxide dehydrogenase as a catalytically competent intermediate in the pathway of acetyl-coenzyme-A synthesis. *J. Biol. Chem. 266*, 20687–20693.
28. Maynard, E. L., and Lindahl, P. A. (1999) Evidence of a molecular tunnel connecting the active sites for CO_2 reduction and acetyl-CoA synthesis in acetyl-CoA synthase from *Clostridium thermoaceticum*. *J. Am. Chem. Soc. 121*, 9221–9222.
29. Elliott, J. I., and Ljungdahl, L. G. (1982) Isolation and characterization of an Fe8-S8 ferredoxin (ferredoxin-II) from *Clostridium thermoaceticum*. *J. Bacteriol. 151*, 328–333.
30. Ragsdale, S. W., and Wood, H. G. (1985) Acetate biosynthesis by acetogenic bacteria—Evidence that carbon-monoxide dehydrogenase is the condensing enzyme that catalyzes the final steps of the synthesis. *J. Biol. Chem. 260*, 3970–3977.
31. Raybuck, S. A., Bastian, N. R., Ormejohnson, W. H., and Walsh, C. T. (1988) Kinetic characterization of the carbon-monoxide acetyl-CoA (carbonyl group) exchange activity of the acetyl-CoA synthesizing Co dehydrogenase from *Clostridium thermoaceticum*. *Biochemistry 27*, 7698–7702.
32. Lundie, L. L., Jr., and Drake, H. L. (1984) Development of a minimally defined medium for the acetogen *Clostridium thermoaceticum*. *J. Bacteriol. 159*, 700–703.
33. Segel, I. H. (1975) Enzyme kinetics: behavior and analysis of rapid equilibrium and steady state enzyme systems, p xxii, 957 pp, Wiley, New York.
34. Harder, S. R., Feinberg, B. A., and Ragsdale, S. W. (1989) A spectroelectrochemical cell designed for low temperature electron paramagnetic resonance titration of oxygen-sensitive proteins. *Anal. Biochem. 181*, 283–287.
35. Hinckley, G. T., and Frey, P. A. (2006) An adaptable spectroelectrochemical titrator: the midpoint reduction potential of the iron-sulfur center in lysine 2,3-aminomutase. *Anal. Biochem. 349*, 103–111.
36. Prince, R. C., and Adams, M. W. W. (1987) Oxidation-reduction properties of the 2Fe4S4 clusters in *Clostridium pasteurianum* ferredoxin. *J. Biol. Chem. 262*, 5125–5128.
37. Wilson, G. S. (1978) Determination of oxidation-reduction potentials. *Methods Enzymol. 54*, 396–410.
38. Dorweiler, J. S., Finke, R. G., and Matthews, R. G. (2003) Cobalamin-dependent methionine synthase: probing the role of the axial base in catalysis of methyl transfer between methyltetrahydrofolate and exogenous cob(I)alamin or cob(I)inamide. *Biochemistry 42*, 14653–14662.
39. Gao-Sheridan, H. S., Pershad, H. R., Armstrong, F. A., and Burgess, B. K. (1998) Discovery of a novel ferredoxin from *Azotobacter vinelandii* containing two [4Fe-4S] clusters with widely differing and very negative reduction potentials. *J. Biol. Chem. 273*, 5514–5519.
40. Green, A. J., Munro, A. W., Cheesman, M. R., Reid, G. A., von Wachenfeldt, C., and Chapman, S. K. (2003) Expression, purification and characterisation of a *Bacillus subtilis* ferredoxin: a potential electron transfer donor to cytochrome P450 BioI. *J. Inorg. Biochem. 93*, 92–99.
41. Yang, S. S., Ljungdahl, L. G., and Legall, J. (1977) 4-iron, 4-sulfide ferredoxin with high thermostability from *Clostridium thermoaceticum*. *J. Bacteriol. 130*, 1084–1090.
42. Kyritsis, P., Hatzfeld, O. M., Link, T. A., and Moulis, J. M. (1998) The two [4Fe-4S] clusters in *Chromatium vinosum* ferredoxin have largely different reduction potentials. Structural origin and functional consequences. *J. Biol. Chem. 273*, 15404–15411.
43. Guerrini, O., Burlat, B., Leger, C., Guigliarelli, B., Soucaille, P., and Girbal, L. (2008) Characterization of two 2[4Fe4S] ferredoxins from *Clostridium acetobutylicum*. *Curr. Microbiol. 56*, 261–267.
44. Mathews, R., Charlton, S., Sands, R. H., and Palmer, G. (1974) On the nature of the spin coupling between the iron-sulfur clusters in the eight-iron ferredoxins. *J. Biol. Chem. 249*, 4326–4328.
45. Mathews, R., Charlton, S., Sands, R. H., and Palmer, G. (1974) Nature of spin coupling between iron-sulfur clusters in 8-iron ferredoxins. *J. Biol. Chem. 249*, 4326–4328.
46. Saeki, K., Jain, M. K., Shen, G. J., Prince, R. C., and Zeikus, J. G. (1989) Purification and properties of ferredoxin and rubredoxin from *Butyribacterium methylotrophicum*. *J. Bacteriol. 171*, 4736–4741.
47. Shanmugasundaram, T., and Wood, H. G. (1992) Interaction of ferredoxin with carbon monoxide dehydrogenase from *Clostridium thermoaceticum*. *J. Biol. Chem. 267*, 897–900.
48. Ragsdale, S. W., Wood, H. G., and Antholine, W. E. (1985) Evidence that an iron-nickel-carbon complex is formed by reaction of CO with the CO dehydrogenase from *Clostridium thermoaceticum*. *Proc. Natl. Acad. Sci. U.S.A. 82*, 6811–6814.
49. Lindahl, P. A., Ragsdale, S. W., and Münck, E. (1990) Mössbauer studies of CO dehydrogenase from *Clostridium thermoaceticum*. *J. Biol. Chem. 265*, 3880–3888.
50. Xia, J. Q., Hu, Z. G., Popescu, C. V., Lindahl, P. A., and Munck, E. (1997) Mossbauer and EPR study of the Ni-activated alpha-subunit of carbon monoxide dehydrogenase from *Clostridium thermoaceticum*. *J. Am. Chem. Soc. 119*, 8301–8312.
51. Kumar, M., and Ragsdale, S. W. (1992) Characterization of the CO binding site of carbon monoxide dehydrogenase from *Clostridium thermoaceticum* by infrared spectroscopy. *J. Am. Chem. Soc. 114*, 8713–8715.
52. Gencic, S., and Grahame, D. A. (2003) Nickel in subunit beta of the acetyl-CoA decarbonylase/synthase multienzyme complex in methanogens: catalytic properties and evidence for a binuclear Ni-Ni site. *J. Biol. Chem. 278*, 6101–6110.
53. Bramlett, M. R., Tan, X., and Lindahl, P. A. (2003) Inactivation of acetyl-CoA synthase/carbon monoxide dehydrogenase by copper. *J. Am. Chem. Soc. 125*, 9316–9317.
54. Schenker, R. P., and Brunold, T. C. (2003) Computational studies on the A cluster of acetyl-coenzyme A synthase: geometric and electronic properties of the NiFeC species and mechanistic implications. *J. Am. Chem. Soc. 125*, 13962–13963.
55. Lu, W. P., and Ragsdale, S. W. (1991) Reductive activation of the coenzyme-A acetyl-CoA isotopic exchange-reaction catalyzed by carbon-monoxide dehydrogenase from *Clostridium thermoaceticum* and its inhibition by nitrous-oxide and carbon-monoxide. *J. Biol. Chem. 266*, 3554–3564.
56. Bhaskar, B., DeMoll, E., and Grahame, D. A. (1998) Redox-dependent acetyl transfer partial reaction of the acetyl-CoA decarbonylase/synthase complex: kinetics and mechanism. *Biochemistry 37*, 14491–14499.
57. Zehnder, A. J. B., and Wuhrmann, K. (1976) Titanium(III) citrate as a nontoxic oxidation-reduction buffering system for culture of obligate anaerobes. *Science 194*, 1165–1166.
58. Furdui, C., and Ragsdale, S. W. (2002) The roles of coenzyme A in the pyruvate:ferredoxin oxidoreductase reaction mechanism: rate enhancement of electron transfer from a radical intermediate to an iron-sulfur cluster. *Biochemistry 41*, 9921–9937.
59. Gencic, S., and Grahame, D. A. (2008) Two separate one-electron steps in the reductive activation of the a cluster in subunit beta of the ACDS complex in *Methanosarcina thermophila*. *Biochemistry 47*, 5544–5555.
60. Tan, X., Surovtsev, I. V., and Lindahl, P. A. (2006) Kinetics of CO insertion and acetyl group transfer steps, and a model of the acetyl-CoA synthase catalytic mechanism. *J. Am. Chem. Soc. 128*, 12331–12338.
61. Barondeau, D. P., and Lindahl, P. A. (1997) Methylation of carbon monoxide dehydrogenase from *Clostridium thermoaceticum* and mechanism of acetyl coenzyme A synthesis. *J. Am. Chem. Soc. 119*, 3959–3970.